# Cu Pad Surface Height Evaluation Technique by In-line SEM for Wafer Hybrid Bonding

Hiroaki Kasai[a], Mayuka Osaki[a],
Kazuhisa Hasumi[b], Nobuyuki Mise[c], Maki Tanaka[b],
Bensu Tunca Altintas[d], Soon Aik Chew[d], Janusz Bogdanowicz[d], Alain Moussa[d], Mohamed Saib[d],
Boyao Zhang[d], and Anne-Laure Charley[d]

[a]Hitachi, Ltd., 292 Yoshidacho, Yokohama, Kanagawa, Japan 244–0817
[b]Hitachi High-Tech Corporation, 552-53 Shinkocho, Hitachinaka, Ibaraki, Japan 312–8504
[c]Hitachi High-Tech Corporation, 1-17-1 Toranomon, Minato, Tokyo, Japan 105–6409
[d]Interuniversity Microelectronics Centre, Kapeldreef 75 B-3001, Leuven, Belgium

## ABSTRACT

Wafer-to-wafer hybrid bonding is a key technology for achieving high-density three-dimensional interconnections in semiconductor devices. This technology directly bonds Cu pads formed on the surface of two wafers, where the surface height of the Cu pad compared to the SiCN surrounding the Cu pad have to be within a few nm. We have developed a method to measure the Cu pad surface height with sub-nm precision by using a top-view scanning electron microscope image. The proposed method is based on the physical principle that the difference in the backscattered electron (BSE) signals of the opposing detectors is dependent on the slope. It estimates the slope of the target with the BSE signal and then calculates the height of the target on the basis of this slope. We compared the Cu pad height measurement results by this method with those by atomic force microscopy and found that ours provided measurement precision on the sub-nm order and demonstrated the capability for evaluation of layout dependency and intra-wafer distribution. Because of its speed and alignment capability, our proposed method is promising for Cu height control in wafer-to-wafer hybrid bonding.

**Keywords:** In-line SEM, hybrid bonding, Cu pad, height evaluation, height measurement

## 1. INTRODUCTION

Wafer-to-wafer hybrid bonding is a key technology for achieving high-density three-dimensional interconnections in semiconductor devices. Its applications have recently expanded to include image sensors and memory packages. This technology directly bonds Cu pads formed on the surface of two wafers (Fig. 1.1), where the bonding surface of the two wafers are polished by chemical mechanical polishing (CMP), activated by plasma, bonded together, and then annealed to increase the bonding strength. The width and pitch of Cu pads currently applied to devices are sub-µm and a few µ m, respectively, and in the near future, the size is expected to be even smaller [1]. When the three-dimensional shape on the surface of a Cu pad is inappropriate, the bonding quality is degraded due to void defects after bonding [2]. To avoid this, the height gap between the surface of the Cu pad and the SiCN surrounding the Cu pad have to be controlled to within a few nm [2]. This means that measuring the surface height of the Cu pads with sub-nm precision is required. The height, which is controlled by CMP, tends to vary depending on the density of the pads and the position intra-wafer [3]. To control the height intra-chip and intra-wafer, it is also necessary to measure a sufficient amount to identify the height distribution intra-chip and intra-wafer.

The scanning electron microscope (SEM) is a wafer measurement and inspection tool that is commonly utilized to measure pattern width, review defects on a wafer, and so on. SEM can take images with a field of view of 10 µm and the resolution of a few nm, both of which are enough for Cu pad evaluation. Therefore, we have developed a height measurement method for the Cu pad surface using SEM images. The challenge is how to obtain height information from top-view SEM images.

Metrology, Inspection, and Process Control XXXVIII, edited by Matthew J. Sendelbach,
Nivea G. Schuch, Proc. of SPIE Vol. 12955, 129551N · © 2024 SPIE
0277-786X · doi: 10.1117/12.3008658

Another wafer height measurement tool is atomic force microscopy (AFM), which mechanically scans the probe near the surface of the target so that it can measure the height of the target directly. However, the mechanical scan is slower than the operation by SEM.

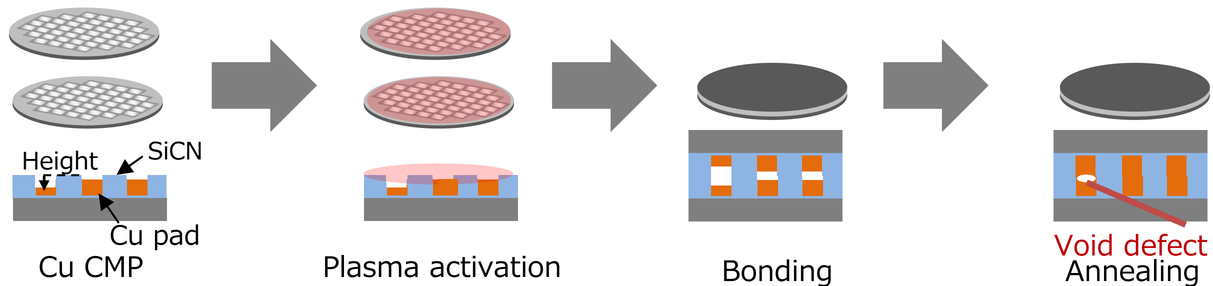


Fig. 1.1 Wafer hybrid bonding process.

## 2. PROPOSED METHOD

SEM captures images by irradiating an electron beam onto the target surface and detecting the scattered electrons. The image signal provides different information on the structure of the target depending on the detection conditions. The measurement target in this paper is the surface height of the Cu pad. As mentioned above, the height and the width are a few nm and sub-µm, respectively, so the aspect ratio is small. Therefore, we examine the use of azimuthally detected shallow-angle backscattered electron (BSE) images, which are assumed to be effective in evaluating the height of low-aspect samples. A schematic diagram of 4-azimuth detectors and example images of each detector are shown in Fig. 2.1(b) and (c). The images are captured by GS1000 (Hitachi High-Tech). We call these detectors NEWS (North, East, West, South) detectors, and they each capture images at the same time. In Fig. 2.1(c), the images exhibit different shadowing at the height boundaries.

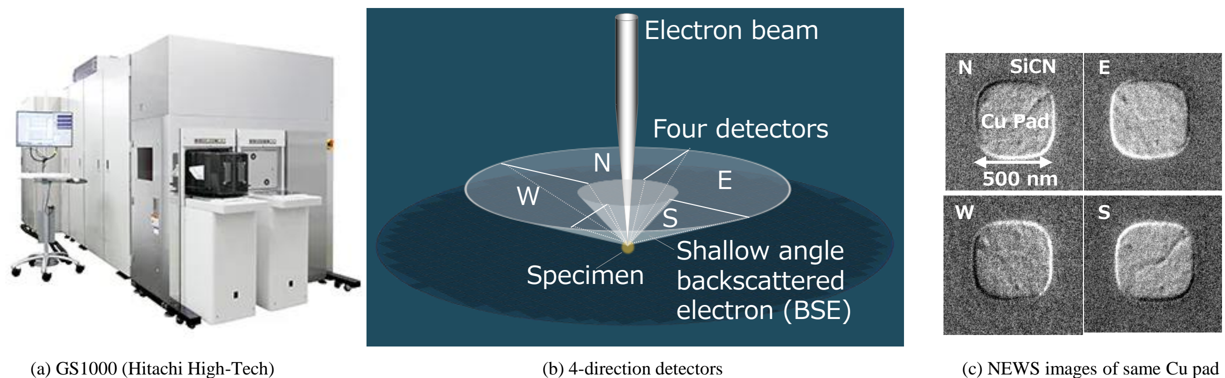


(a) GS1000 (Hitachi High-Tech) (b) 4-direction detectors (c) NEWS images of same Cu pad

Fig. 2.1 Schematic diagram of SEM imaging and 4-direction detector.

The proposed height measurement method is inspired by the imaging principle. When an electron beam irradiates an object, the signal intensity detected by the NEWS detector varies depending on the slope angle of the object. A schematic diagram of the signal profile of each detector is shown Fig. 2.2. When an electron beam irradiates a flat area, such as Point A, BSEs are emitted symmetrically. Therefore, the signal intensities detected by the opposing detectors, West and East, are the same. In contrast, when an electron beam irradiates a sloped area, such as Point B, BSEs are emitted more in the west direction than in the east direction. Therefore, the signal intensity detected by the West detector is larger than that detected by the East detector. Accordingly, when the right edge of the Cu pad is dark in an east image, the Cu pad is recessed, and conversely, when the right edge is bright, the Cu pad protrudes (Fig. 2.3). Thus, recess and protrusion can be distinguished.

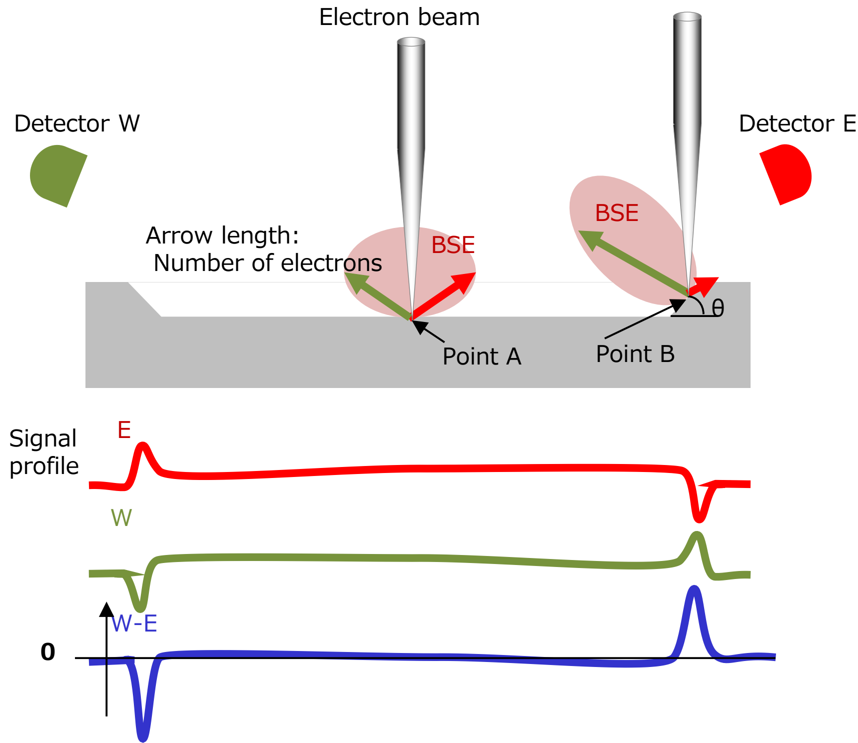


Fig. 2.2 Relationship between BSE signal and slope angle.

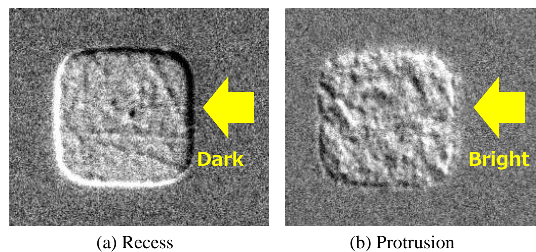


(a) Recess (b) Protrusion

Fig. 2.3 Recess and protrusion pad images of East detector.

To quantify the Cu pad height, we focused on the difference in signal between the opposing detectors (Fig. 2.2). At the flat area, the difference in signal between the West and East detector is zero. At the sloped area, the difference is physically formulated as proportional to the sine function of the slope angle [4][5]. The derivation is as follows(see Fig. 2.4)

If the scattering distribution of emitted electrons follows Lambert's distribution, the signal amount $S$ can be expressed by

$$\frac{dS}{d\theta} \propto cos\theta, \tag{1}$$

where $\theta$ is the slope angle at the electron irradiation point and is the side wall angle in Fig. 2.2 and Fig. 2.4.

By integrating equation (1), the signal amount of detectors E and W, $S_E$ and $S_W$, can be expressed by

$$S_E = \sigma(\theta)(1 + \sin\theta)/2 \,,\; S_W = \sigma(\theta)(1 - \sin\theta)/2, \tag{2}$$

where $\sigma(\theta)$ is the yield of each detector.

In the case of BSE, $\sigma(\theta)$ is proportional to $cos^m\theta$ (0<m<0.5). When $\theta$ is less than 60 degrees, it can be approximated by a constant value[5]. Although details are omitted, AFM measurements shows that the side wall angle $\theta$ of Cu pad is small. Therefore, equation (2) can be approximated by

$$S_E = \sigma(1 + \sin\theta)/2\ ,\ S_W = \sigma(1 - \sin\theta)/2. \tag{3}$$

The difference between $S_E$ and $S_W$ can be expressed as

$$S_W - S_E \propto sin\theta. \tag{4}$$

The difference in signal amount between opposing detectors is proportional to the slope angle $\theta$ at the irradiation position.

The height between two points is expressed by the integral of the tangent function of the slope angle $\theta$. If $\theta$ is small, it can be approximated by the integral of the sine function of $\theta$. Then, the height between two points can be expressed by

$$Height = \int \alpha(S_W - S_E)\, dx. \tag{5}$$

In this paper, we define the height of the Cu pad as the surface height of the pad at its center compared to outside of the pad. Since the pad has edges in two directions, east-west and north-south, the average of the height calculated in each direction is defined as the height index of the pad, expressed by

$$Height\ index = \left\{\int_{x_1}^{x_c}(S_W - S_E)dx + \int_{y_1}^{y_c}(S_N - S_S)dy\right\}/2$$
$$\text{[<0 for recess, >0 for protrusion]}, \tag{6}$$

where the coordinate at the center of the pad is $(x_c, y_c)$ and the coordinates outside the pad for the east-west and north-south directions are $(x_1, y_c)$ and $(x_1, y_c)$, respectively.

The height index in Eq. (6) is positive in the case of recess and negative in the case of protrusions. In principle, the height index should be proportional to the height of the Cu pad.

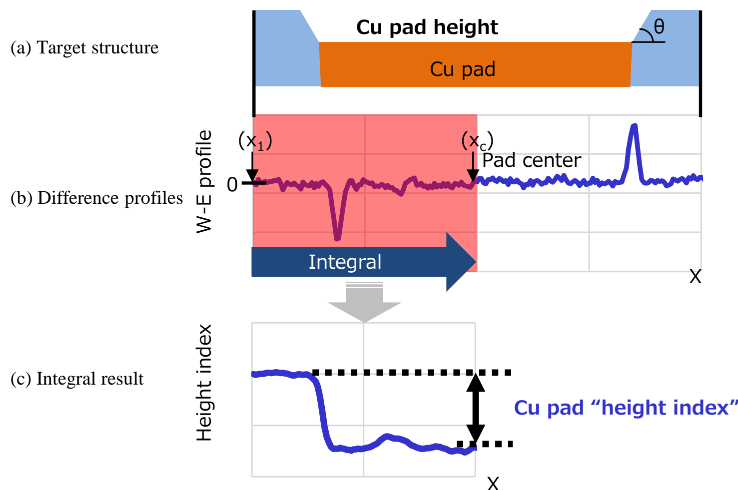


Fig. 2.4 Height index.

## 3. EVALUATION METHOD AND CONDITIONS

We examined the capability of the proposed height index through three experiments evaluating the sensitivity of the height index, the layout dependence, and the intra-wafer distribution. The height index is compared to the AFM measurement results as a reference.

Fig. 3.1 shows information on the samples used in this evaluation. In (a), multiple chips are formed on the wafer surface. In (b), there are many Cu pads on the chip, as well as some blank areas where there are no pads. In (c), the width of the Cu pad is 500 nm, the pitch is 1 μm, and the height varies from –7 nm to +1 nm. The details of the three experimental conditions are provided in Table 3.1.

The purpose of experiment 1 is to evaluate the sensitivity of the height index. Here, we compared the height index by SEM to the measurement value by AFM for each pad. To obtain height variations, three wafers with different CMP conditions were prepared, and seven chips were selected horizontally and vertically within a wafer. Then, 42 images were taken for each chip. Fig. 3.2(a) shows the location of the seven chips on the wafers and the location of the 42 images on the chips. The height index was calculated for each pad on the SEM images. AFM measured the height as the difference in height between the center area of the Cu pad and the surrounding area of the pad, as shown in Fig. 3.3. Alignment marks on the chips (e.g., the T-mark in Fig. 3.2(a)) allows a comparison of SEM and AFM measurement results of the same pad.

The purpose of experiment 2 is to evaluate the layout dependence of the Cu pad height. Since the amount of CMP polishing depends on the pattern density, we investigated whether the proposed height index can evaluate the pattern density dependence. For one chip from experimental data 1, both the height index and the height measured by AFM are mapped on the layout.

The purpose of experiment 3 is to evaluate the intra-wafer distribution of the Cu pad height. The height uniformity is also degraded intra-wafer by processes such as deposition, CMP, and so on. For evaluation of intra-wafer distribution, we increased the number of evaluation points on a wafer. As shown in Fig. 3.2(b), 55 chips were imaged on a wafer, and one image was taken for each chip. The average height index of 64 pads in one image was compared to the average height of 64 to 121 pads measured by AFM. In other words, the pads measured by SEM and AFM were not exactly the same. We evaluated the intra-wafer distribution on two wafers.

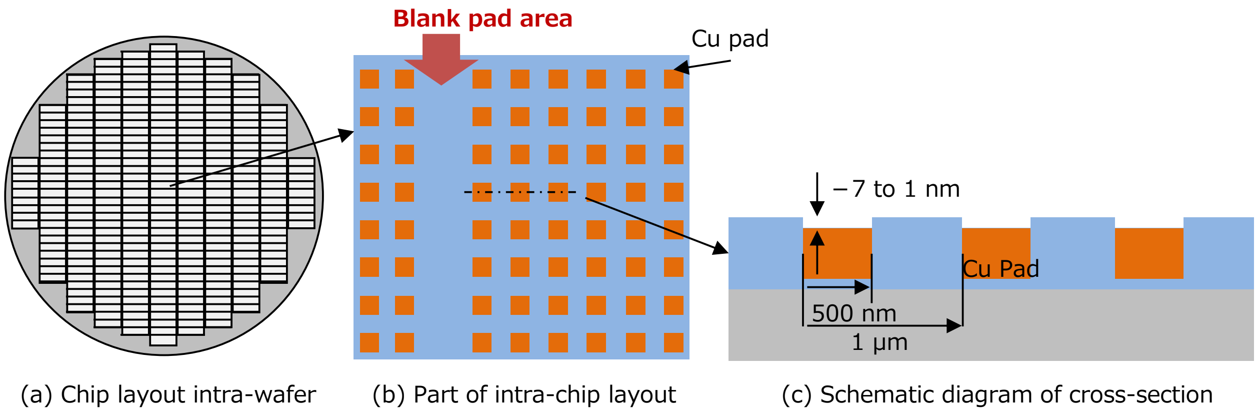


Fig. 3.1 Sample information.

Table 3.1 Experimental conditions.

| Experiment | Evaluation item | The number of wafers | The number of chips per wafer | The number of images per chip |
|---|---|---|---|---|
| 1 | Sensitivity | 3 | 7 | 42 |
| 2 | Layout dependence | 1 | 1 | |
| 3 | Intra-wafer distribution | 2 | 55 | 1 |

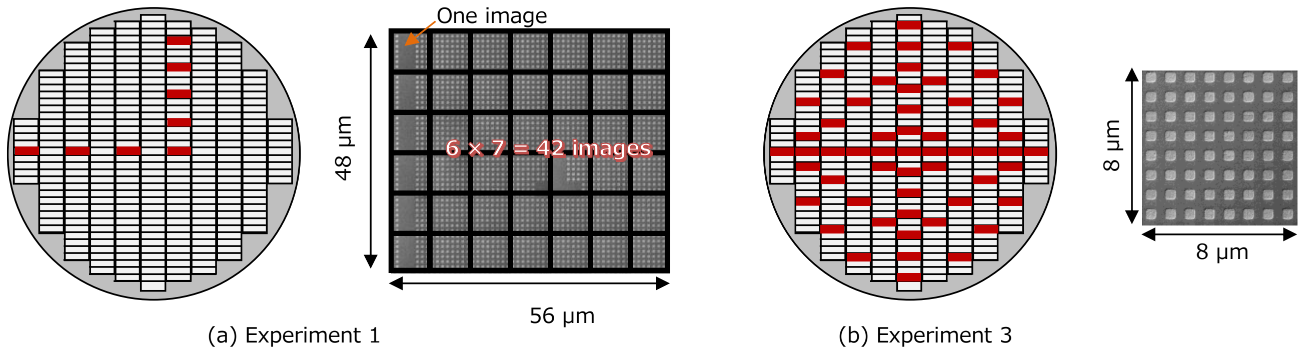


Fig. 3.2 Imaging area.

Table 3.2 SEM conditions.

| Acceleration voltage | 500 V |
|---|---|
| Probe current | 550 pA |
| Field of view | 8 µm |
| Pixel size | 3.91 nm/pixel |

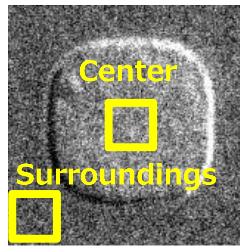


Fig. 3.3 AFM height measurement area.

## 4. RESULTS AND DISCUSSION

### 4.1 Experiment 1: Sensitivity evaluation

The results of experiment 1 are shown in Fig. 4.1(a), where the vertical axis indicates the height index with SEM [a.u.] and the horizontal axis is the height measured with AFM [nm]. These results show that the height index is sensitive to height variation. The units of the height index are converted to nm based on the fitting line in Fig. 4.1(a), and the results are shown in Fig. 4.1(b). Here, the vertical axis of the graph is the height measured by SEM [nm]. The measurement error is calculated as the root mean squared error (RMSE) using Eq. (7). The error here is 0.42 nm, which includes the measurement error of AFM and the effect of the difference of measurement area between SEM and AFM.

The above findings suggest that measurement is possible with a measurement error of 0.42 nm. However, wafer 1 exhibits a different trend compared to wafers 2 and 3, as shown in Fig. 4.1(a). To clarify what caused this difference, we investigate the following hypothesis. Fig. 4.2 shows examples of the East detector image on each wafer. The signal profile for each image is also overlaid, and schematic diagrams of the cross-sectional shape of each wafer are shown in the same figure. The cross-sectional shape is confirmed by AFM measurements, and the signal profile depends on the cross-sectional shape. Since convex shape causes dark peaks of the signal at the convex edges, wafers 2 and 3 are considered to have a convex shape, whereas wafer 1 has a flat bottom. Such differences in shape may cause the difference in the trends. In the derivation of the height index, the tangent function is approximated by the sine function of $\theta$, assuming $\theta$ is small in Eq. (5). Different shapes may cause different amounts of approximation error, thus explaining the different trends.

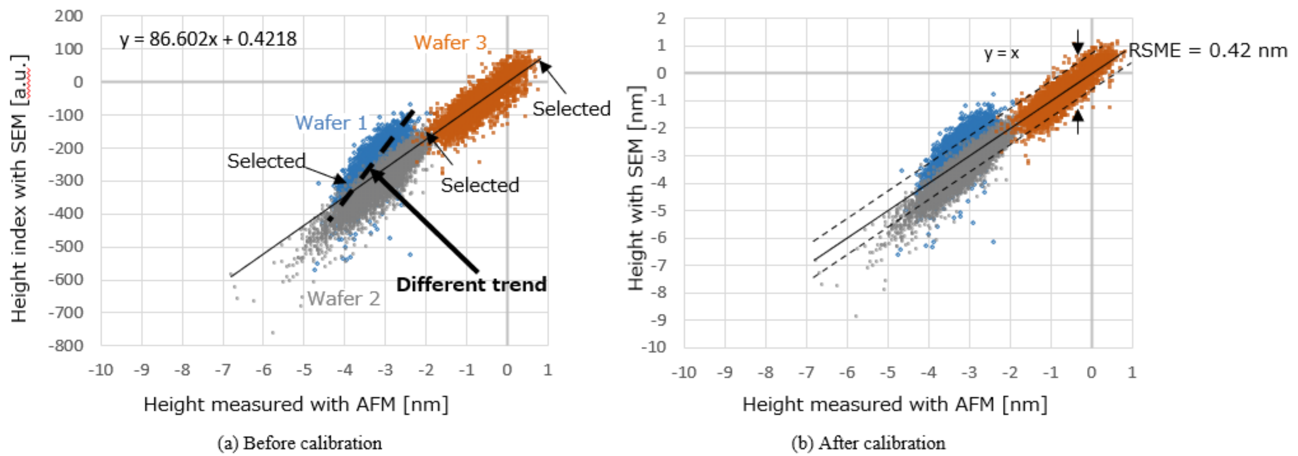


Fig. 4.1 Results of sensitivity evaluation.

$$RMSE = \sqrt{\frac{1}{n}\sum_{i=0}^{n-1}(y_i - y_{i0})^2} \tag{7}$$

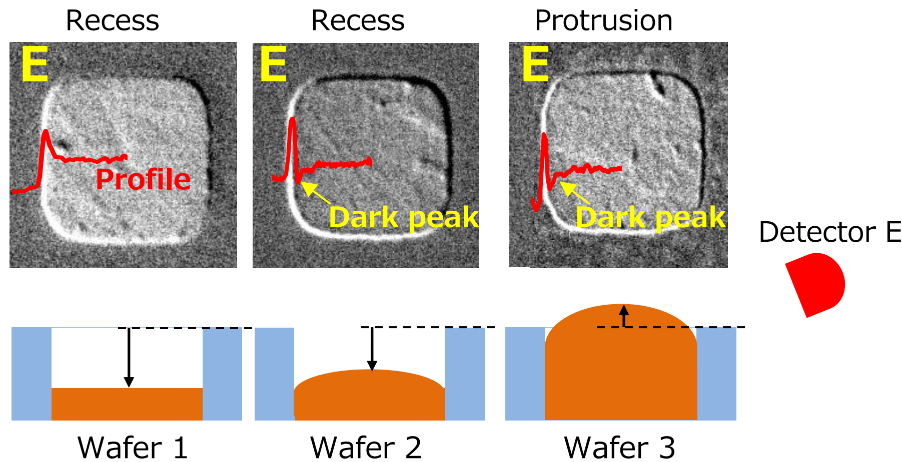


Fig. 4.2 Selected Cu pad images from East detector.

## 4.2 Experiment 2: Layout dependence

Fig. 4.3 shows the results of the evaluation of layout dependence of the Cu pad height. The horizontal and vertical axes of the graph are coordinates. Each plot indicates the location of the measured pad. The pitch of the pads was 1 µm. The color of the plot indicates the height. Fig. 4.3 (a) is the height measured by proposed method with SEM. The field of view of SEM is 8 µm, so it takes 42 images on a chip. SEM sets the imaging position so that the pads do not overlap the edges of the image. However, the positioning error sometimes causes measurement errors at the periphery of the image since the position of $x_1$ or $y_1$ outside of the pad in Eq. (6) is not included in the image. Such missing pads are not plotted on the graph. We expect that the number of missing pads can be reduced by improving the image capturing method and measurement algorithm. Fig. 4.3(b) is the height measured by AFM. The trend of layout dependence by SEM is similar to that of AFM. In particular, the surface height of the pad becomes lower at low-density area, where there are no pads at the left side of the graph in Fig. 4.3. These results demonstrate the capability of the proposed method for evaluating the layout dependence of the Cu pad height.

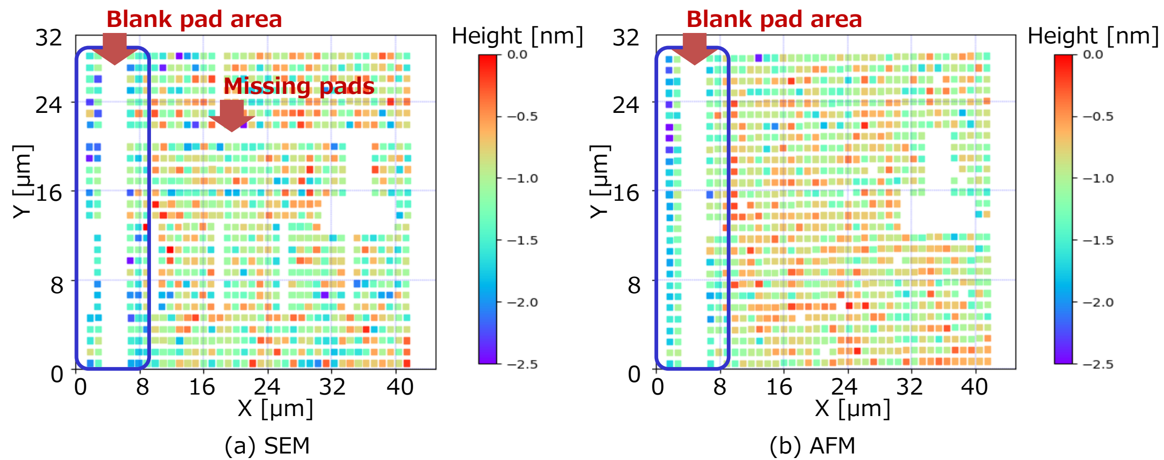

Fig. 4.3 Results of layout dependence evaluation.

### 4.3 Experiment 3: Evaluation of intra-wafer distribution

Fig. 4.4 shows the results of the evaluation of the intra-wafer distribution of the Cu pad height. The horizontal and vertical axes of the graph indicate the chip number on the wafer. Each plot shows the position of the measured chip, and the color indicates the height. In this example, SEM was able to evaluate the intra-wafer distribution eight times faster than AFM. The trend of intra-wafer distribution measured by SEM is similar to that of AFM. Wafer 1 shows a concentric variation in height distribution, whereas wafer 3 shows a gradual increase in height from left to right. Intra-chip variations, defined as the standard deviation of the height measured by SEM, are 0.31 nm and 0.34 nm in wafers 1 and 3, respectively. This indicates that if only one pad is measured, differences of less than 0.31 nm and 0.34 nm cannot be detected for wafers 1 and 3. Smaller difference can be detected by averaging the height on multiple pads. High-speed imaging by SEM is advantageous for more sensitive evaluation of intra-wafer distribution of the Cu pad height. These findings demonstrate the capability of the proposed method for evaluating intra-wafer distribution of the Cu pad height.

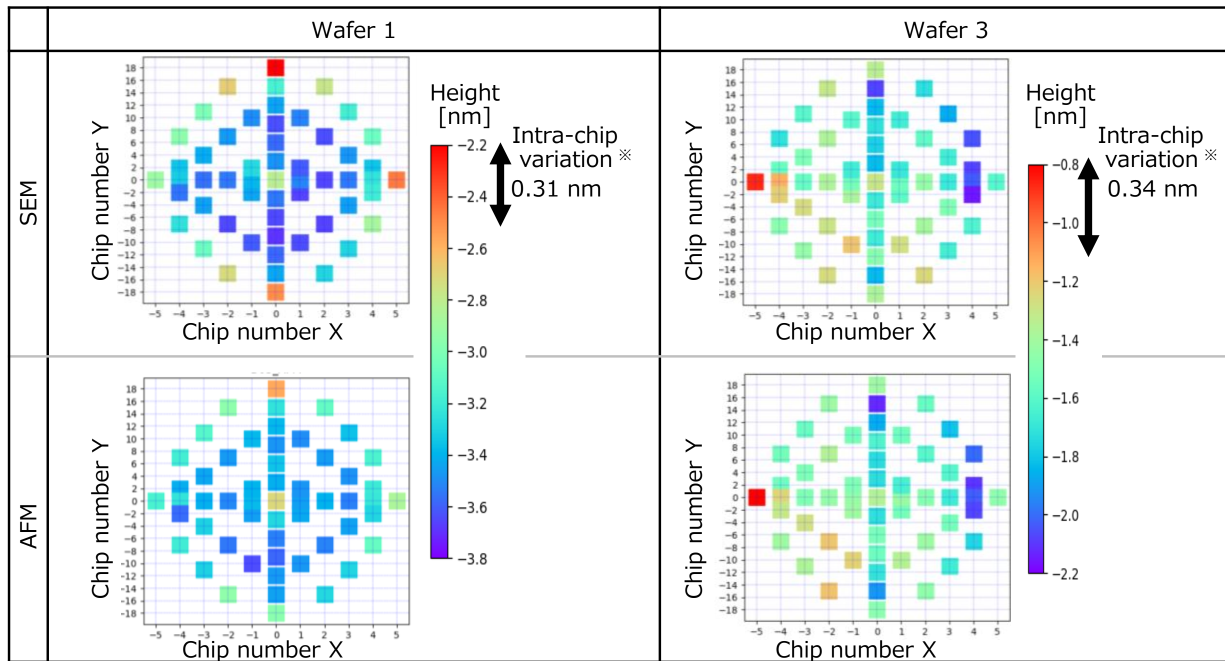

Fig. 4.4 Results of intra-wafer distribution evaluation.

## 5. CONCLUSION

We have developed a method to measure Cu pad height by SEM with four-directional BSE detectors. The proposed method is based on the physical principle that the difference in the BSE signals of the opposing detectors is dependent on the slope: specifically, it estimates the slope of the target with the BSE signal and calculates the height of the target with this slope. We compared the Cu pad height measurement results by our method with those by AFM and found that ours provided measurement precision on the sub-nm order and demonstrated the capability for evaluation of layout dependency and intra-wafer distribution. Because of its speed and alignment capability, our proposed method is promising for Cu height control in wafer-to-wafer hybrid bonding.

## REFERENCES


[1] S. B. Samavedam *et al.*, "Future Logic Scaling: Towards Atomic Channels and Deconstructed Chips," *2020 IEEE International Electron Devices Meeting (IEDM)*, San Francisco, CA, USA, 2020, pp. 1.1.1-1.1.10, doi: 10.1109/IEDM13553.2020.9372023.

[2] J. De Messemaeker *et al.*, "New Cu “Bulge-Out” Mechanism Supporting SubMicron Scaling of Hybrid Wafer-to-Wafer Bonding," *2023 IEEE 73rd Electronic Components and Technology Conference (ECTC)*, Orlando, FL, USA, 2023, pp. 109-113, doi: 10.1109/ECTC51909.2023.00027.

[3] Chidambaram, Vivek et al. “Wafer Level Fine-Pitch Hybrid Bonding: Challenges and Remedies.” 2020 IEEE 22nd Electronics Packaging Technology Conference (EPTC) (2020): 459-463.

[4] M. Lange, L. Reimer, and C. Tollkamp, “Testing of detector strategies in scanning electron microscopy by isodensities,” Journal of Microscopy, vol. 134, pt. 1, April 1984, pp. 1–12.

[5] L. Reimer, R. Bongeler, and V. Dessai, “Shape from Shading Using Multiple Detector Signals in Scanning Electron Microscopy,” Scanning Microscopy, vol. 1, no. 3, 1987, pp. 963–973.